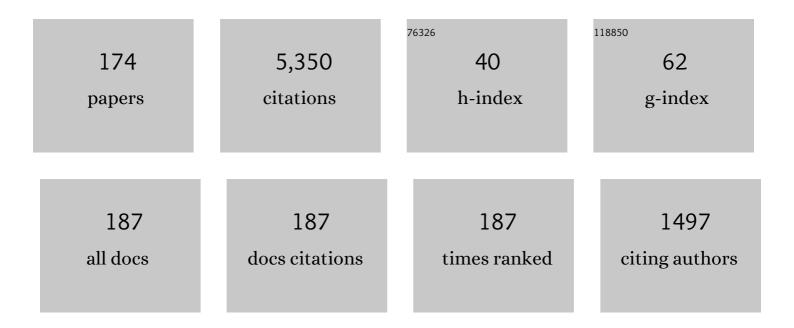
List of Publications by Year in descending order

Source: https://exaly.com/author-pdf/3761849/publications.pdf Version: 2024-02-01



#	Article	IF	CITATIONS
1	Interfacial reactions between magnesia refractory and electric arc furnace (EAF) slag with use of direct reduced iron (DRI) as raw material. Ceramics International, 2022, 48, 4526-4538.	4.8	10
2	Effect of pyro-processing conditions on impurity removal and precious metal enrichment in waste printed circuit board (WPCB) recycling process. Resources, Conservation and Recycling, 2022, 179, 106068.	10.8	6
3	Effect of Temperature on the Oxidation Behavior of Al and Ti in Inconel® 718 Alloy by ESR Slag with Different Amounts of CaO. Jom, 2022, 74, 1228-1236.	1.9	2
4	Oxidation behavior of boron in 9CrMoCoB steel by CaF2–CaO–Al2O3–SiO2–B2O3 electroslag remelting (ESR) type slag. Journal of Materials Research and Technology, 2022, 17, 574-585.	5.8	7
5	Effect of temperature on the slag/refractory interfacial reaction with directed reduced iron (DRI) addition in an electric arc furnace (EAF) process: Diffusional growth of magnesiowüstite layer by Boltzmann-Matano analysis. Ceramics International, 2022, 48, 17217-17224.	4.8	2
6	Desulfurization behavior of Si-killed 316L stainless steel melt by CaO-SiO2-CaF2-Al2O3-MgO slag. Journal of Materials Research and Technology, 2022, 18, 2250-2260.	5.8	6
7	Inclusion Engineering in Medium Mn Steels: Effect of Hot-Rolling Process on the Deformation Behaviors of Oxide and Sulfide Inclusions. Metallurgical and Materials Transactions B: Process Metallurgy and Materials Processing Science, 2022, 53, 2182-2197.	2.1	7
8	Influence of Al2O3 and SiO2 on the structure and viscosity of iron-compound bearing calcium-aluminosilicate slags. Journal of Alloys and Compounds, 2022, 916, 165328.	5.5	6
9	Effect of slag composition on the distribution and separation behavior of arsenic between CaO-based slag and liquid copper. Journal of Hazardous Materials, 2022, 436, 129154.	12.4	5
10	Effect of Physicochemical Properties of Slag on the Removal Rate of Alumina Inclusions in the Ruhrstahl–Heraeus (RH) Refining Conditions. Metallurgical and Materials Transactions B: Process Metallurgy and Materials Processing Science, 2022, 53, 2523-2533.	2.1	3
11	Comparison of Oxidation Behavior of Various Reactive Elements in Alloys during Electroslag Remelting (ESR) Process: An Overview. ISIJ International, 2022, 62, 1561-1572.	1.4	2
12	Gold Solubility in CaO-SiO2-Al2O3-Fe2O3 Slags. Jom, 2021, 73, 688-693.	1.9	1
13	Interfacial Reactions and Inclusion Formations at an Early Stage of FeNb Alloy Additions to Molten Iron. ISIJ International, 2021, 61, 209-218.	1.4	6
14	Viscosity-Structure Relationship of CaO–Al ₂ O ₃ –Fe _t O–SiO <sub> Ruhrstahl-Heraeus (RH) Refining Slags. ISIJ International, 2021, 61, 724-733.</sub> 	;2& l t#sub&	>j â€ "MgO
15	Role of recrystallization and second phases on mechanical properties of (CoCrFeMnNi)95.2Al3.2Ti1.6 high entropy alloy. Materials Science & Engineering A: Structural Materials: Properties, Microstructure and Processing, 2021, 814, 141249.	5.6	11
16	Interfacial Phenomena and Inclusion Formation Behavior at Early Melting Stages of HCFeCr and LCFeCr Alloys in Liquid Iron. Metallurgical and Materials Transactions B: Process Metallurgy and Materials Processing Science, 2021, 52, 2459-2473.	2.1	6
17	Non-metallic Inclusions in Different Ferroalloys and Their Effect on the Steel Quality: A Review. Metallurgical and Materials Transactions B: Process Metallurgy and Materials Processing Science, 2021, 52, 2892-2925.	2.1	32
18	Effect of fluorspar on the interfacial reaction between electric arc furnace slag and magnesia refractory: Competitive corrosion-protection mechanism of magnesiowüstite layer. Ceramics International, 2021, 47, 20387-20398.	4.8	12

#	Article	IF	CITATIONS
19	Effect of Oxygen Blowing on Copper Droplet Formation and Emulsification Phenomena in the Converting Process. Journal of Sustainable Metallurgy, 2021, 7, 831-847.	2.3	2
20	Effect of Industrial Waste Fluxes (Red Mud and White Mud) on Dephosphorization and Refractory Corrosion: Applications to Electric Arc Furnace Process Using Direct Reduced Iron. Metallurgical and Materials Transactions B: Process Metallurgy and Materials Processing Science, 2021, 52, 3583-3595.	2.1	3
21	Effect of Slag Composition on Dephosphorization and Foamability in the Electric Arc Furnace Steelmaking Process: Improvement of Plant Operation. Metallurgical and Materials Transactions B: Process Metallurgy and Materials Processing Science, 2021, 52, 3613-3623.	2.1	5
22	Evolution of the Non-metallic Inclusions Influenced by Slag-Metal Reactions in Ti-Containing Ferritic Stainless Steel. Metallurgical and Materials Transactions B: Process Metallurgy and Materials Processing Science, 2021, 52, 3986-4001.	2.1	3
23	Effect of LCFeCr Alloy Additions on the Non-metallic Inclusion Characteristics in Ti-Containing Ferritic Stainless Steel. Metallurgical and Materials Transactions B: Process Metallurgy and Materials Processing Science, 2021, 52, 3815-3832.	2.1	9
24	Inclusion engineering in Co-based duplex entropic alloys. Materials and Design, 2021, 210, 110097.	7.0	14
25	Effect of White Mud Addition on Desulfurization Rate of Molten Steel. Metallurgical and Materials Transactions B: Process Metallurgy and Materials Processing Science, 2021, 52, 3596.	2.1	5
26	Desulfurization Behavior of Incoloy® 825 Superalloy by CaO-Al2O3-MgO-TiO2 Slag. Metallurgical and Materials Transactions B: Process Metallurgy and Materials Processing Science, 2021, 52, 3660-3670.	2.1	6
27	Influence of slag composition and oxygen potential on thermodynamic behavior of vanadium in FeO-TiO2-MgO-SiO2-Al2O3 smelting slag and molten iron. Journal of Materials Research and Technology, 2021, 15, 5723-5732.	5.8	1
28	Effect of Tundish Flux on Compositional Changes in Non-metallic Inclusions in Stainless Steel Melts. ISIJ International, 2021, 61, 2998-3007.	1.4	7
29	Structural Understanding of MnO–SiO2–Al2O3–Ce2O3 Slag via Raman, 27Al NMR and X-ray Photoelectron Spectroscopies. Metals and Materials International, 2020, 26, 1872-1880.	3.4	21
30	Strengthening of ultrafine-grained equiatomic CoCrFeMnNi high-entropy alloy by nitrogen addition. Materials Letters, 2020, 258, 126772.	2.6	18
31	Investigation on the precipitate formation and behavior in nitrogen-containing equiatomic CoCrFeMnNi high-entropy alloy. Materials Letters, 2020, 258, 126806.	2.6	16
32	Influence of calcium aluminate flux on reoxidation behaviour of molten steel during continuous casting process. Ironmaking and Steelmaking, 2020, 47, 84-92.	2.1	11
33	Effect of CaF2 on Phosphorus Refining from Molten Steel by Electric Arc Furnace Slag using Direct Reduced Iron (DRI) as a Raw Material. Metallurgical and Materials Transactions B: Process Metallurgy and Materials Processing Science, 2020, 51, 3028-3038.	2.1	14
34	Kinetic Modeling of Nonmetallic Inclusions Behavior in Molten Steel: A Review. Metallurgical and Materials Transactions B: Process Metallurgy and Materials Processing Science, 2020, 51, 2453-2482.	2.1	41
35	Influence of Manufacturing Conditions on Inclusion Characteristics and Mechanical Properties of FeCrNiMnCo Alloy. Metals, 2020, 10, 1286.	2.3	18
36	Distribution characteristics of inclusions along with the surface sliver defect on the exposed panel of automobile: A quantitative electrolysis method. International Journal of Minerals, Metallurgy and Materials, 2020, 27, 1489-1498.	4.9	11

#	Article	IF	CITATIONS
37	Thermodynamics of iron redox equilibria and viscosity-structure relationship of CaO Al2O3FetO melts. Journal of Non-Crystalline Solids, 2020, 542, 120089.	3.1	16
38	Effect of Fluorspar and Industrial Wastes (Red Mud and Ferromanganese Slag) on Desulfurization Efficiency of Molten Steel. Metallurgical and Materials Transactions B: Process Metallurgy and Materials Processing Science, 2020, 51, 2309-2320.	2.1	16
39	Prediction of Inclusion Evolution During Refining and Solidification of Steel: Computational Simulation and Experimental Confirmation. Metallurgical and Materials Transactions B: Process Metallurgy and Materials Processing Science, 2020, 51, 1211-1224.	2.1	20
40	Mechanism of Improving Heat-Affected Zone Toughness of Steel Plate with Mg Deoxidation after High-Heat-Input Welding. Metals, 2020, 10, 162.	2.3	8
41	Mechanical Performance Improvement by Nitrogen Addition in N-CoCrNi Compositionally Complex Alloys. Metallurgical and Materials Transactions A: Physical Metallurgy and Materials Science, 2020, 51, 3228-3237.	2.2	11
42	Observations of FeO Reduction in Electric Arc Furnace Slag by Aluminum Black Dross: Effect of CaO Fluxing on Slag Morphology. Metallurgical and Materials Transactions B: Process Metallurgy and Materials Processing Science, 2020, 51, 1201-1210.	2.1	11
43	Improving the production efficiency of high-titania slag in Ti extraction process: fluxing effect on formation of pseudobrookite. Scientific Reports, 2020, 10, 6530.	3.3	5
44	Massive Recycling of Waste Mobile Phones: Pyrolysis, Physical Treatment, and Pyrometallurgical Processing of Insoluble Residue. ACS Sustainable Chemistry and Engineering, 2019, 7, 14119-14125.	6.7	29
45	Mechanism of MgO dissolution in MgF2–CaF2–MF (M=Li or Na) melts: Kinetic analysis via in-situ high temperature confocal scanning laser microscopy (HT-CSLM). Ceramics International, 2019, 45, 20251-20257.	4.8	10
46	Precipitate behavior in nitrogen-containing CoCrNi medium-entropy alloys. Materials Characterization, 2019, 157, 109888.	4.4	41
47	Assessment of Physicochemical Properties of Electrical Arc Furnace Slag and Their Effects on Foamability. Metallurgical and Materials Transactions B: Process Metallurgy and Materials Processing Science, 2019, 50, 2959-2968.	2.1	8
48	Influence of Exposure Temperature on Degradation of Magnesia Refractory by Steel Refining Slags. Metals and Materials International, 2019, 25, 1360-1365.	3.4	8
49	Influence of Temperature on Reaction Mechanism of Ilmenite Ore Smelting for Titanium Production. Metallurgical and Materials Transactions B: Process Metallurgy and Materials Processing Science, 2019, 50, 1830-1840.	2.1	10
50	Effect of nitrogen on grain growth and formability of Ti-stabilized ferritic stainless steels. Scientific Reports, 2019, 9, 6369.	3.3	12
51	Viscosityâ€structure relationship of alkaline earth silicate melts containing manganese oxide and calcium fluoride. Journal of the American Ceramic Society, 2019, 102, 4943-4955.	3.8	24
52	Evolution of Oxide Inclusions in Si-Mn-Killed Steel During Protective Atmosphere Electroslag Remelting. Metallurgical and Materials Transactions B: Process Metallurgy and Materials Processing Science, 2019, 50, 1139-1147.	2.1	32
53	Crystallization and vitrification behavior of CaO-SiO2-FetO-Al2O3 slag: Fundamentals to use mineral wastes in production of glass ball. Journal of Cleaner Production, 2019, 225, 743-754.	9.3	22
54	Interfacial reaction between magnesia refractory and "FeO―rich slag: Formation of magnesiowüstite layer. Ceramics International, 2019, 45, 10481-10491.	4.8	26

#	Article	IF	CITATIONS
55	Influence of Aluminum-Carbon Composite Pellets on FeO Reduction and Iron Recovery from Electric Arc Furnace Slag. Metallurgical and Materials Transactions B: Process Metallurgy and Materials Processing Science, 2019, 50, 903-913.	2.1	5
56	Use of Industrial Waste (Al-Dross, Red Mud, Mill Scale) as Fluxing Agents in the Sulfurization of Fe-Ni-Cu-Co Alloy by Carbothermic Reduction of Calcium Sulfate. Metallurgical and Materials Transactions B: Process Metallurgy and Materials Processing Science, 2018, 49, 939-943.	2.1	3
57	Influence of CaF2 in calcium aluminate-based slag on the degradation of magnesia refractory. Ceramics International, 2018, 44, 13197-13204.	4.8	24
58	Manganese Recovery by Silicothermic Reduction of MnO in BaO-MnO-MgO-CaF2 (-SiO2) Slags. Metallurgical and Materials Transactions B: Process Metallurgy and Materials Processing Science, 2018, 49, 514-518.	2.1	11
59	Formation Mechanism of Oxide-Sulfide Complex Inclusions in High-Sulfur-Containing Steel Melts. Metallurgical and Materials Transactions B: Process Metallurgy and Materials Processing Science, 2018, 49, 311-324.	2.1	28
60	Effect of CaO/Al ₂ O ₃ Ratio of Ladle Slag on Formation Behavior of Inclusions in Mn and V Alloyed Steel. ISIJ International, 2018, 58, 88-97.	1.4	26
61	Synergistic Effect of Nitrogen and Refractory Material on TiN Formation and Equiaxed Grain Structure of Ferritic Stainless Steel. Metallurgical and Materials Transactions B: Process Metallurgy and Materials Processing Science, 2018, 49, 877-893.	2.1	24
62	Effect of Direct Reduced Iron (DRI) on Dephosphorization of Molten Steel by Electric Arc Furnace Slag. Metallurgical and Materials Transactions B: Process Metallurgy and Materials Processing Science, 2018, 49, 3381-3389.	2.1	16
63	Characterization of non-metallic inclusions and their influence on the mechanical properties of a FCC single-phase high-entropy alloy. Journal of Alloys and Compounds, 2018, 763, 546-557.	5.5	59
64	Refractory–Slag–Metal–Inclusion Multiphase Reactions Modeling Using Computational Thermodynamics: Kinetic Model for Prediction of Inclusion Evolution in Molten Steel. Metallurgical and Materials Transactions B: Process Metallurgy and Materials Processing Science, 2017, 48, 46-59.	2.1	63
65	Novel design of ferronickel smelting slag by utilizing red mud as a fluxing agent: Thermochemical computations and experimental confirmation. Calphad: Computer Coupling of Phase Diagrams and Thermochemistry, 2017, 56, 185-195.	1.6	5
66	Effect of Rice Husk Ash Insulation Powder on the Reoxidation Behavior of Molten Steel in Continuous Casting Tundish. Metallurgical and Materials Transactions B: Process Metallurgy and Materials Processing Science, 2017, 48, 1736-1747.	2.1	29
67	Thermochemical analysis for the reduction behavior of FeO in EAF slag via Aluminothermic Smelting Reduction (ASR) process: Part II. Effect of aluminum dross and lime fluxing on Fe and Mn recovery. Calphad: Computer Coupling of Phase Diagrams and Thermochemistry, 2017, 58, 229-238.	1.6	15
68	Thermochemical analysis for the reduction behavior of FeO in EAF slag via Aluminothermic Smelting Reduction (ASR) process: Part Ι. Effect of aluminum on Fe & Mn recovery. Calphad: Computer Coupling of Phase Diagrams and Thermochemistry, 2017, 58, 219-228.	1.6	14
69	Effect of Slag Chemistry on the Desulfurization Kinetics in Secondary Refining Processes. Metallurgical and Materials Transactions B: Process Metallurgy and Materials Processing Science, 2017, 48, 2123-2135.	2.1	26
70	Method of recycling titanium scraps via the electromagnetic cold crucible technique coupled with calcium treatment. Journal of Alloys and Compounds, 2017, 727, 931-939.	5.5	18
71	Modification of Inclusions in Molten Steel by Mg-Ca Transfer from Top Slag: Experimental Confirmation of the â€ ⁻ Refractory-Slag-Metal-Inclusion (ReSMI)â€ ^{-™} Multiphase Reaction Model. Metallurgical and Materials Transactions B: Process Metallurgy and Materials Processing Science, 2017. 48, 2820-2825.	2.1	41
72	Vitrification of red mud with mine wastes through melting and granulation process – Preparation of glass ball. Journal of Non-Crystalline Solids, 2017, 475, 129-135.	3.1	25

#	Article	IF	CITATIONS
73	Inclusions in Stainless Steels â^ A Review. Steel Research International, 2017, 88, 1700130.	1.8	105
74	Corrosion-erosion behavior of MgAl2O4 spinel refractory in contact with high MnO slag. Ceramics International, 2017, 43, 15074-15079.	4.8	22
75	Effect of Initial Iron Content in a Zinc Bath on the Dissolution Rate of Iron During a Hot Dip Galvanizing Process. Metallurgical and Materials Transactions A: Physical Metallurgy and Materials Science, 2017, 48, 1788-1796.	2.2	1
76	Distribution Behavior of Aluminum and Titanium Between Nickel-Based Alloys and Molten Slags in the Electro Slag Remelting (ESR) Process. Metallurgical and Materials Transactions B: Process Metallurgy and Materials Processing Science, 2017, 48, 2147-2156.	2.1	21
77	TEM characterization of a TiN-MgAl2O4 epitaxial interface. Journal of Alloys and Compounds, 2017, 695, 476-481.	5.5	24
78	Relationship Between Sulfide Capacity and Structure of MnO-SiO2-Al2O3-Ce2O3 System. Metallurgical and Materials Transactions B: Process Metallurgy and Materials Processing Science, 2017, 48, 545-553.	2.1	19
79	Sulfurization of Fe-Ni-Cu-Co Alloy to Matte Phase by Carbothermic Reduction of Calcium Sulfate. Metallurgical and Materials Transactions B: Process Metallurgy and Materials Processing Science, 2016, 47, 1103-1112.	2.1	22
80	Effect of Energy Input on the Characteristic of AISI H13 and D2 Tool Steels Deposited by a Directed Energy Deposition Process. Metallurgical and Materials Transactions A: Physical Metallurgy and Materials Science, 2016, 47, 2529-2535.	2.2	44
81	EffectÂof Physicochemical Properties of Slag and Flux on the Removal Rate of Oxide Inclusion from Molten Steel. Metallurgical and Materials Transactions B: Process Metallurgy and Materials Processing Science, 2016, 47, 3225-3230.	2.1	31
82	Recovery of iron and removal of hazardous elements from waste copper slag via a novel aluminothermic smelting reduction (ASR) process. Journal of Cleaner Production, 2016, 137, 777-787.	9.3	85
83	Effect of Halide Flux on Physicochemical Properties of MgCl2-Based Molten Salts for Accelerating Zirconium Production: Thermodynamic Assessment. Metallurgical and Materials Transactions E, 2016, 3, 218-226.	0.5	0
84	Initial Wetting and Spreading Rates Between SiC and CaO-SiO2-MnO Slag. Metallurgical and Materials Transactions B: Process Metallurgy and Materials Processing Science, 2016, 47, 1832-1838.	2.1	14
85	Understanding Sulfide Capacity of Molten Aluminosilicates via Structural Information from â€~Raman' and â€~NMR' Spectroscopic Methodologies. , 2016, , 715-721.		0
86	Thermodynamic Stability of Spinel Phase at the Interface Between Alumina Refractory and CaO–CaF ₂ –SiO ₂ –Al ₂ O ₃ –MgO–MnO Slags. Jour the American Ceramic Society, 2015, 98, 1974-1981.	nalsos	29
87	Influence of Refractory-Steel Interfacial Reaction on the Formation Behavior of Inclusions in Ce-containing Stainless Steel. ISIJ International, 2015, 55, 2589-2596.	1.4	58
88	Variation in the Chemical Driving Force for Intragranular Nucleation in the Multi-pass Weld Metal of Ti-Containing High-Strength Low-Alloy Steel. Metallurgical and Materials Transactions A: Physical Metallurgy and Materials Science, 2015, 46, 3581-3591.	2.2	20
89	Influence of CaF2 on the Viscosity and Structure of Manganese Ferroalloys Smelting Slags. Metallurgical and Materials Transactions B: Process Metallurgy and Materials Processing Science, 2015, 46, 741-748.	2.1	31
90	Diffusion coefficient of gaseous zirconium tetrachloride (ZrCl4). Fluid Phase Equilibria, 2015, 389, 4-8.	2.5	1

#	Article	IF	CITATIONS
91	Thermodynamics of Indium Dissolution Behavior in FeO-Bearing Metallurgical Slags. Metallurgical and Materials Transactions B: Process Metallurgy and Materials Processing Science, 2015, 46, 235-242.	2.1	15
92	Effect of CaF2 Addition on the Silicothermic Reduction of MnO in Ferromanganese Slag. Metallurgical and Materials Transactions B: Process Metallurgy and Materials Processing Science, 2015, 46, 1154-1161.	2.1	20
93	Thermodynamics of Gold Dissolution Behavior in CaO-SiO2-Al2O3-MgOsat Slag System. Metallurgical and Materials Transactions B: Process Metallurgy and Materials Processing Science, 2015, 46, 2449-2457.	2.1	23
94	Influence of the oxygen partial pressure and the boron content on the behavior of boron in calcium silicate melts. Journal of Non-Crystalline Solids, 2015, 429, 54-60.	3.1	4
95	Structure-Viscosity Relationship of Low-silica Calcium Aluminosilicate Melts. ISIJ International, 2014, 54, 2031-2038.	1.4	139
96	Effect of Al deoxidation on the formation behavior of inclusions in Ce-added stainless steel melts. Metals and Materials International, 2014, 20, 959-966.	3.4	33
97	Effect of Mg–Ti Deoxidation on the Formation Behavior of Equiaxed Crystals During Rapid Solidification of Iron Alloys. Steel Research International, 2014, 85, 1303-1309.	1.8	53
98	Isothermal and non-isothermal sublimation kinetics of zirconium tetrachloride (ZrCl4) for producing nuclear grade Zr. Materials Chemistry and Physics, 2014, 143, 1075-1081.	4.0	9
99	Influence of Ti on non-metallic inclusion formation and acicular ferrite nucleation in high-strength low-alloy steel weld metals. Metals and Materials International, 2014, 20, 119-127.	3.4	63
100	Effect of Slag Composition on the Concentration of Al2O3 in the Inclusions in Si-Mn-killed Steel. Metallurgical and Materials Transactions B: Process Metallurgy and Materials Processing Science, 2014, 45, 953-960.	2.1	63
101	Mn-Depleted Zone Formation in Rapidly Cooled High-Strength Low-Alloy Steel Welds. Metallurgical and Materials Transactions A: Physical Metallurgy and Materials Science, 2014, 45, 4753-4757.	2.2	23
102	Oxide Formation Mechanisms in High Manganese Steel Welds. Metallurgical and Materials Transactions A: Physical Metallurgy and Materials Science, 2014, 45, 2046-2054.	2.2	25
103	Viscosity-Structure Relationship in the CaO-SiO2-MnO-CaF2 Slag for the Production of Manganese Ferroalloys. , 2014, , 605-612.		Ο
104	Effect of silicate structure on thermodynamic properties of calcium silicate melts: Quantitative analysis of Raman spectra. Metals and Materials International, 2013, 19, 577-584.	3.4	49
105	Effect of CaO Addition on Iron Recovery from Copper Smelting Slags by Solid Carbon. Metallurgical and Materials Transactions B: Process Metallurgy and Materials Processing Science, 2013, 44, 1352-1363.	2.1	103
106	Structure–Property Relationship of CaO-MgO-SiO2 Slag: Quantitative Analysis of Raman Spectra. Metallurgical and Materials Transactions B: Process Metallurgy and Materials Processing Science, 2013, 44, 938-947.	2.1	67
107	Competitive Dissolution Mechanism of Sulfur in CaMnSilicate Melts: Structural View. Steel Research International, 2013, 84, 664-669.	1.8	19
108	Conversion of Calcium Phosphide to Calcium Phosphate in Reducing Dephosphorization Slags by Oxygen Injection. ISIJ International, 2013, 53, 2266-2268.	1.4	11

#	Article	IF	CITATIONS
109	Effect of CaF2 Addition on the Viscosity and Structure of CaO–SiO2–MnO Slags. ISIJ International, 2013, 53, 958-965.	1.4	64
110	Thermodynamics for the Influence of Slag Composition on the Inclusion Control in Semi-Killed Liquid Steels. , 2013, , 207-211.		2
111	Effect of Atmosphere and Slag Composition on the Evolution of PH3 Gas during Cooling of Reducing Dephosphorization Slags. ISIJ International, 2013, 53, 385-390.	1.4	7
112	Morphologies of Alumina Nano- and Microparticles at the Fe/Al2O3 Interface and the Effects of Reaction Time and Substrate Roughness on Size Distribution. ISIJ International, 2013, 53, 547-549.	1.4	3
113	Structure^ ^ndash;Property Correlations of CaO^ ^ndash;SiO2^ ^ndash;MnO Slag Derived from Raman Spectroscopy. ISIJ International, 2012, 52, 1627-1636.	1.4	107
114	Effect of Slag Composition on the Distribution Behavior of Pb between FetO-SiO2 (-CaO, Al2O3) Slag and Molten Copper. Metallurgical and Materials Transactions B: Process Metallurgy and Materials Processing Science, 2012, 43, 1098-1105.	2.1	32
115	Composition–structure–property relationships of CaO–MO–SiO2 (M=Mg2+, Mn2+) systems derived from micro-Raman spectroscopy. Journal of Non-Crystalline Solids, 2012, 358, 3096-3102.	3.1	60
116	Thermodynamics of Reducing Refining of Phosphorus from Si-Mn Alloy Using CaO-CaF2 Slag. Metallurgical and Materials Transactions B: Process Metallurgy and Materials Processing Science, 2012, 43, 1243-1246.	2.1	15
117	Effect of Complex Inclusion Particles on the Solidification Structure of Fe-Ni-Mn-Mo Alloy. Metallurgical and Materials Transactions B: Process Metallurgy and Materials Processing Science, 2012, 43, 1550-1564.	2.1	75
118	Sulfide Capacity of CaO–SiO ₂ –MnO–Al ₂ O <sub& Slags at 1873 K. ISIJ International, 2012, 52, 764-769.</sub& 	& g #3</s	su is >&am
119	Sulfide Capacity and Excess Free Energy of CaO^ ^ndash;SiO2^ ^ndash;MnO Slag Derived from Structural Analysis of Raman Spectra. ISIJ International, 2012, 52, 2303-2304.	1.4	21
120	Metastable Phases of Dross Particles Formed in a Molten Zinc Bath and Prediction of Soluble Aluminum During Galvannealing Processes. Metallurgical and Materials Transactions A: Physical Metallurgy and Materials Science, 2012, 43, 1934-1943.	2.2	6
121	Characterization of Nonmetallic Inclusions in High-Manganese and Aluminum-Alloyed Austenitic Steels. Metallurgical and Materials Transactions A: Physical Metallurgy and Materials Science, 2012, 43, 2316-2324.	2.2	79
122	Dissolution Mechanism of Indium in CaO-Al2O3-SiO2 Slag at Low Silica Region. Metallurgical and Materials Transactions B: Process Metallurgy and Materials Processing Science, 2012, 43, 440-442.	2.1	16
123	Interfacial Reaction Between CaO-SiO2-MgO-Al2O3 Flux and Fe-xMn-yAl (xÂ=Â10 and 20 mass pct, yÂ=Â1, 3, and and Materials Processing Science, 2012, 43, 875-886.) Tj ETQq1 2.1	1 0.78431 56
124	Influence of Aluminum on the Formation Behavior of Zn-Al-Fe Intermetallic Particles in a Zinc Bath. Metallurgical and Materials Transactions A: Physical Metallurgy and Materials Science, 2012, 43, 195-207.	2.2	16
125	Effect of inclusions on the solidification structures of ferritic stainless steel: Computational and experimental study of inclusion evolution. Calphad: Computer Coupling of Phase Diagrams and Thermochemistry, 2011, 35, 455-462.	1.6	86
126	Sulfide Capacity of the CaO–SiO2–MnO Slag at 1873 K. ISIJ International, 2011, 51, 1375-1382.	1.4	49

#	Article	IF	CITATIONS
127	On the Dissolution Behavior of Sulfur in Ternary Silicate Slags. Metallurgical and Materials Transactions B: Process Metallurgy and Materials Processing Science, 2011, 42, 1211-1217.	2.1	42
128	Dissolution Behavior of Indium in CaO-SiO2-Al2O3 Slag. Metallurgical and Materials Transactions B: Process Metallurgy and Materials Processing Science, 2011, 42, 1224-1230.	2.1	30
129	Solubility of Nitrogen in High Manganese Steel (HMnS) Melts: Interaction Parameter between Mn and N. Metallurgical and Materials Transactions B: Process Metallurgy and Materials Processing Science, 2011, 42, 1081-1085.	2.1	26
130	Control of MgO·Al2O3 Spinel Inclusions in Stainless Steels. ISIJ International, 2010, 50, 1333-1346.	1.4	317
131	Hot Metal Desulfurization by CaO–SiO2–CaF2–Na2O Slag Saturated with MgO. ISIJ International, 2010, 50, 215-221.	1.4	29
132	The effect of boron oxide on the crystallization behavior of MgAl2O4 spinel phase during the cooling of the CaO-SiO2-10 mass.% MgO-30 mass.%Al2O3 systems. Metals and Materials International, 2010, 16, 987-992.	3.4	21
133	In situ observation of the dissolution phenomena of SiC particle in CaO–SiO2–MnO slag. Journal of the European Ceramic Society, 2010, 30, 3181-3186.	5.7	53
134	Interfacial Reaction between Refractory Materials and Metallurgical Slags containing Fluoride. Steel Research International, 2010, 81, 860-868.	1.8	45
135	Carbide Capacity of CaO–SiO2–MnO Slag for the Production of Manganese Alloys. ISIJ International, 2010, 50, 1078-1083.	1.4	36
136	Thermodynamics of Copper Dissolution into MnO–SiO2–MnS Inclusion System. ISIJ International, 2009, 49, 171-177.	1.4	5
137	Thermodynamics of Titanium Oxide in CaO–SiO2–Al2O3–MgOsatd–CaF2 Slag Equilibrated with Fe–11mass%Cr Melt. ISIJ International, 2009, 49, 337-342.	1.4	35
138	Diffusion Kinetics of Oxygen in β-Titanium Measured by Molten Flux Method. Metallurgical and Materials Transactions A: Physical Metallurgy and Materials Science, 2009, 40, 495-498.	2.2	6
139	Phase diagram study for the CaO-SiO2-Cr2O3-5 mass.%MgO-10 mass.%MnO system. Metals and Materials International, 2009, 15, 677-681.	3.4	31
140	Corrosion Behaviors of Zirconia Refractory by CaO–SiO ₂ –MgO–CaF ₂ Slag. Journal of the American Ceramic Society, 2009, 92, 717-723.	3.8	51
141	Electrochemical Method for Controlling the Interfacial Oxygen in Molten Fe with ZrO2 Based Solid Electrolyte. ISIJ International, 2009, 49, 1882-1888.	1.4	18
142	Novel Approach to Link between Viscosity and Structure of Silicate Melts via Darken's Excess Stability Function: Focus on the Amphoteric Behavior of Alumina. Metallurgical and Materials Transactions B: Process Metallurgy and Materials Processing Science, 2008, 39, 150-153.	2.1	75
143	Thermodynamics of the Formation of MgO-Al2O3-TiO x Inclusions in Ti-Stabilized 11Cr Ferritic Stainless Steel. Metallurgical and Materials Transactions B: Process Metallurgy and Materials Processing Science, 2008, 39, 853-861.	2.1	77
144	Thermodynamic investigation on the formation of inclusions containing MgAl2O4 spinel during 16Cr–14Ni austenitic stainless steel manufacturing processes. Materials Science & Engineering A: Structural Materials: Properties, Microstructure and Processing, 2008, 472, 43-51.	5.6	71

#	Article	IF	CITATIONS
145	Formation of CaZrO3 at the interface between CaO–SiO2–MgO–CaF2(–ZrO2) slags and magnesia refractories: Computational and experimental study. Calphad: Computer Coupling of Phase Diagrams and Thermochemistry, 2007, 31, 149-154.	1.6	30
146	Solidification structure of CaO–SiO2–MgO–Al2O3Â(–CaF2) systems and computational phase equilibria: Crystallization of MgAl2O4 spinel. Calphad: Computer Coupling of Phase Diagrams and Thermochemistry, 2007, 31, 428-437.	1.6	35
147	Formation Mechanism of Spinel-Type Inclusions in High-Alloyed Stainless Steel Melts. Metallurgical and Materials Transactions B: Process Metallurgy and Materials Processing Science, 2007, 38, 657-663.	2.1	83
148	Discussion on "The Estimation of the Iso-viscosity Lines in Molten CaF2-CaO-SiO2 System". ISIJ International, 2007, 47, 1368-1369.	1.4	25
149	Effect of ZrO ₂ Addition to the CaO-SiO ₂ -MgO-CaF ₂ Slags on the Sulfur Removal from the 16Cr-14Ni Stainless Steel Melts. Materials Transactions, 2006, 47, 2038-2043.	1.2	15
150	Solidification Behavior of Calcium Aluminosilicate Melts Containing Magnesia and Fluorspar. Journal of the American Ceramic Society, 2006, 89, 608-615.	3.8	32
151	Effect of ferrosilicon addition on the composition of inclusions in 16Cr-14Ni-Si stainless steel melts. Metallurgical and Materials Transactions B: Process Metallurgy and Materials Processing Science, 2006, 37, 791-797.	2.1	72
152	Inclusion control of ferritic stainless steel by aluminum deoxidation and calcium treatment. Metallurgical and Materials Transactions B: Process Metallurgy and Materials Processing Science, 2005, 36, 67-73.	2.1	87
153	Effect of CaO-Al2O3-MgO slags on the formation of MgO-Al2O3 inclusions in ferritic stainless steel. Metallurgical and Materials Transactions B: Process Metallurgy and Materials Processing Science, 2005, 36, 495-502.	2.1	108
154	Reduction Behavior of EAF Slags Containing Cr2O3 Using Aluminum at 1793 K. ISIJ International, 2004, 44, 790-794.	1.4	20
155	Amphoteric behavior of alumina in viscous flow and structure of CaO-SiO2 (-MgO)-Al2O3 slags. Metallurgical and Materials Transactions B: Process Metallurgy and Materials Processing Science, 2004, 35, 269-275.	2.1	186
156	Effect of fluorspar and alumina on the viscous flow of calcium silicate melts containing MgO. Journal of Non-Crystalline Solids, 2004, 337, 150-156.	3.1	56
157	Thermodynamics of Fluoride Vaporisation from Slags containing CaF ₂ at 1773 K. Steel Research International, 2004, 75, 807-811.	1.8	19
158	Carbide Capacity of CaO-SiO2-CaF2(-Na2O) Slags at 1773 K. ISIJ International, 2004, 44, 223-228.	1.4	18
159	Improvement of the cleanliness of 16% Cr containing ferritic stainless steel in AOD processes. Revue De Metallurgie, 2004, 101, 291-299.	0.3	4
160	FT-IR Spectroscopic Study on Structure of CaO-SiO2 and CaO-SiO2-CaF2 Slags ISIJ International, 2002, 42, 344-351.	1.4	155
161	Structural Investigation of CaO-Al2O3 and CaO-Al2O3-CaF2 Slags via Fourier Transform Infrared Spectra ISIJ International, 2002, 42, 38-43.	1.4	110
162	The effect of CaF2 on the viscosities and structures of CaO-SiO2(-MgO)-CaF2 slags. Metallurgical and Materials Transactions B: Process Metallurgy and Materials Processing Science, 2002, 33, 723-729.	2.1	93

JOO HYUN PARK

#	Article	IF	CITATIONS
163	Thermodynamic behavior of nickel in CaO-SiO2-FetO slag. Metallurgical and Materials Transactions B: Process Metallurgy and Materials Processing Science, 2002, 33, 55-59.	2.1	11
164	Carbide Capacity of CaO-Al2O3-CaF2 Slag at 1773 K ISIJ International, 2002, 42, 127-131.	1.4	7
165	Sulfide Capacity and Phase Equilibria of MnO-TiO2-MnS System at 1723 K ISIJ International, 2001, 41, 1460-1464.	1.4	19
166	Foaming Behavior of CaO-SiO2-FeO-MgOsatd-X (X=Al2O3,MnO, P2O5, and CaF2) Slags at High Temperatures ISIJ International, 2001, 41, 317-324.	1.4	47
167	Thermodynamic behavior of Na2O-B2O3 melt. Metallurgical and Materials Transactions B: Process Metallurgy and Materials Processing Science, 2001, 32, 297-303.	2.1	6
168	Solubility of Silver in MO (M ₂ O)–B ₂ O ₃ (M = Ca,) Tj	ETOQq00	0 ngBT /Over
169	Thermodynamic Behavior of Carbon in Molten Slags. ISIJ International, 2000, 40, S96-S100.	1.4	6
170	Quantitative analysis of the relative basicity of CaO and BaO by silver solubility in slags. Metallurgical and Materials Transactions B: Process Metallurgy and Materials Processing Science, 1999, 30, 689-694.	2.1	28
171	Solubility of carbon in CaO-B2O3 and BaO-B2O3 slags. Metallurgical and Materials Transactions B: Process Metallurgy and Materials Processing Science, 1999, 30, 1045-1052.	2.1	16
172	Thermodynamic study on the effect of CaF ₂ on the nitrogen and carbon solubility in the CaO-Al ₂ O ₃ -CaF ₂ slag system. Steel Research = Archiv Für Das Eisenhüttenwesen, 1999, 70, 215-220.	0.3	7
173	Removal of Pb from Molten Copper by Fe _t O-SiO ₂ (-CaO,) Tj ETQq1 1 0.784314 rgBT /C)verlock 10	D Tf 50 342 T

174 Viscosity-Structure Relationship in the CaO-SiO₂-MnO-CaF₂Slag for the Production of Manganese Ferroalloys. , 0, , 605-612.